Princeton Plasma Physics Laboratory

PPPL- 4743

PPPL- 4743

A Full-wave Model for Wave Propagation and Dissipation in the Inner Magnetosphere Using the Finite Element Method

Ernest Valeo, Jay R. Johnson, Eun-Hwa and Cynthia Phillips

March, 2012

Prepared for the U.S. Department of Energy under Contract DE-AC02-09CH11466.

Princeton Plasma Physics Laboratory
Report Disclaimers

Full Legal Disclaimer

Trademark Disclaimer

PPPL Report Availability

Princeton Plasma Physics Laboratory:

http://www.pppl.gov/techreports.cfm

Office of Scientific and Technical Information (OSTI):

http://www.osti.gov/bridge

Related Links:

U.S. Department of Energy

Office of Scientific and Technical Information

Fusion Links

A Full-wave Model for Wave Propagation and Dissipation in the Inner Magnetosphere using the Finite Element Method

Jay R Johnson, Ernest Valeo, Eun-Hwa Kim, and Cynthia Phillips

Princeton Plasma Physics Laboratory
Princeton University, Princeton NJ 08543-0451

ABSTRACT

A wide variety of plasma waves play an important role in the energization and loss of particles in the inner magnetosphere. Our ability to understand and model wave-particle interactions in this region requires improved knowledge of the spatial distribution and properties of these waves as well as improved understanding of how the waves depend on changes in solar wind forcing and/or geomagnetic activity. To this end, we have developed a two-dimensional, finite element code that solves the full wave equations in global magnetospheric geometry. The code describes three-dimensional wave structure including mode conversion when ULF, EMIC, and whistler waves are launched in a two-dimensional axisymmetric background plasma with general magnetic field topology. We illustrate the capabilities of the code by examining the role of plasmaspheric plumes on magnetosonic wave propagation; mode conversion at the ion-ion and Alfven resonances resulting from external, solar wind compressions; and wave structure and mode conversion of electromagnetic ion cyclotron waves launched in the equatorial magnetosphere, which propagate along the magnetic field lines toward the ionosphere. We also discuss advantages of the finite element method for resolving resonant structures, and how the model may be adapted to include nonlocal kinetic effects.

1. INTRODUCTION

Waves play a key role in the acceleration and loss of radiation belt and ring current particle populations [*Reeves et al.*, 2009; *Thorne*, 2010]. Global ultra low frequency (ULF) modes can be driven externally through solar wind compressions and velocity driven instabilities or internally through drift-bounce resonance with energetic ring current ions. Traditionally, acceleration of radiation belt particles was believed to occur because these large-scale fluctuations allow particles to diffuse radially away from the plasma source region at the inner edge of the plasma sheet into the inner magnetosphere. Such particles experience significant energy gain through betatron acceleration. While numerous studies demonstrate that radial diffusion is real and affects radiation belt structure and dynamics in profound ways, a growing body of evidence indicates that radial diffusion alone cannot explain the full range of radiation belt dynamics. For example, multisatellite observations recently showed that increases in accelerated electrons begin at the center of the radiation belts and not the edges as would be required by diffusion acting alone [*Chen et al.*, 2007]. Such enhancements require local particle acceleration processes. Several other higher frequency wave modes are also thought to be important for electron energization and loss processes. Magnetosonic waves (with frequency around the lower hybrid frequency) and whistler chorus waves may be important for electron acceleration, while plasmaspheric hiss, electromagnetic ion cyclotron waves (EMIC) and whistler chorus are believed to be important for local loss processes by pitch angle scattering. Reduction of energetic particle flux occurs when particles are scattered into the loss cone and precipitate into the ionosphere.

Our ability to understand and model the dynamic variability of the radiation belts and ring current requires improved knowledge of the spatial distribution and properties of the important plasma waves in the magnetosphere and their variability due to changes in either solar wind forcing or geomagnetic activity. Major uncertainties remain, for example, on the spatial distribution and properties of EMIC waves, the spectral properties of equatorial magnetosonic waves, and the wave normal distribution of chorus emissions. To this end, we develop an advanced full wave model based on the finite element method. The model is well suited to address the key science question —what is the spatial distribution, frequency, and polarization of the wave modes that affect radiation belt and ring current dynamics? Currently, our finite element wave model describes three-dimensional wave propagation of

cold plasma waves in a general two-dimensional geometry, and can be used to examine wave distribution and properties.

2. FINITE ELEMENT METHOD

Understanding wave propagation, dissipation and mode conversion processes is also of critical importance in the study of laboratory fusion plasmas, where electromagnetic waves, launched from an antenna at the edge of the magnetically confined plasma, are used to provide control of the local equilibrium temperature and current profiles. Tremendous progress in understanding the dynamics of waves in fusion plasmas has been made in the past decade by utilizing massively parallel computing platforms to directly solve the wave equation in realistic geometry with non-Maxwellian particle distribution functions and without assuming that wavelengths are small relative to the Larmor radius of the ions [*Bonoli et al.*, 2007]. Prior to the use of massively parallel algorithms, it was not possible to retain sufficient spatial resolution in the simulations to model the propagation of both the longer wavelength modes launched by the antenna and the shorter wavelength modes excited in the plasma via mode conversion.

We develop a finite element code appropriate for general geometries using the expertise in modeling radio frequency heating processes. The code currently solves the cold plasma wave equations in two-dimensions as described below.

Assuming time dependence, $\exp(-i\omega t)$, the linear, cold plasma wave equation takes the form:

$$\nabla\times\nabla\times\mathbf{E}-\frac{\omega^2}{c^2}\boldsymbol{\varepsilon}\cdot\mathbf{E}=4\pi i\frac{\omega}{c^2}\mathbf{j}_e \quad (1)$$

where $\mathbf{j}_e$ is the (localized) external current source, which generates the waves within our model. This source could be an instability in the equatorial region excited, for example, by free energy in velocity space, and its structure could be specified from kinetic simulations in the equatorial magnetosphere. Alternatively, the source could be external compressions in the outer magnetosphere that propagate energy into the inner magnetosphere leading to mode conversion at the ion-ion hybrid resonance.

The equation is solved with absorbing (outgoing wave) boundary conditions at the edge of the solution domain. The dielectric tensor

$$\boldsymbol{\varepsilon}=S(\mathbf{I}-\hat{\mathbf{b}}\hat{\mathbf{b}})+iD\mathbf{I}\times\hat{\mathbf{b}}+P\hat{\mathbf{b}}\hat{\mathbf{b}}\,, \quad (2)$$

where *S*, *D*, and *P* are the Stix functions that provide the plasma response [*Stix*, 1992], is naturally expressed in coordinates aligned along and across the local ambient magnetic field direction $\hat{\mathbf{b}} = \mathbf{B}/|\mathbf{B}|$. For an axisymmetric magnetospheric model Eq. (1) is most naturally expressed in cylindrical (*r*, *z*, φ) coordinates, and typically, *P* >> *S*, *D*, with the result that **E** parallel to **B** is much smaller the perpendicular components. In order to accurately capture this disparity, the field is represented in terms of its projections along and perpendicular to **B**. With the assumption that $\mathbf{B} \cdot \hat{\varphi} = 0$, we pick a local, orthogonal basis **b**, φ, and, $\hat{\boldsymbol{\eta}} = \hat{\mathbf{b}} \times \hat{\varphi}$ and write

$$E = \sum_n (E_{b,n}\hat{b} + E_{\eta,n}\hat{\eta} + E_{\phi,n}\hat{\varphi}) \exp in\phi \,. \tag{3}$$

For a two-dimensional axisymmetric quasi-equilibrium modes with different azimuthal mode number do not couple, but they would couple for a general 3D configuration [e.g., *Cheng*, 1995].

Singular field behavior is expected both at hybrid (associated with each pair of species-lower hybrid and ion-ion) and ion cyclotron resonances and at magnetic field lines which support Alfvén eigenmodes or ion-ion hybrid resonance [*Lee et al.*, 2008, *Kim et al.*, 2008a]. Resolution of this singular behavior requires a high density of mesh points normal to the singular lines. In order to adapt to these multiple singular lines, we solve the equation on an unstructured triangular mesh. We represent the variation of the field within each triangle by vertex-based linear finite elements local basis function, $F_{j,k}$, where *j* labels each triangle and *k* = 1, 2, 3 labels each of its vertices. That is, $F_{j,k}$ varies linearly between 1 at vertex k^{th} and 0 at the other vertices, and is identically 0 outside triangle *j*. Thus the electric field may be represented as:

$$E(r,z) = \sum_{j,k} \mathbf{E}_{j,k} F_{j,k}(r,z) \,. \tag{4}$$

Eq. (1) is cast into matrix form by taking its inner product in turn with each $F_{j,k}$, and integrating by parts to obtain the weak variational form [*Brambilla*, 1999, see for example]

$$\int d\phi\, r dr\, dz \{[\nabla \times (\mathbf{F}^*_{j,k} \exp(-in\phi))] \cdot [\nabla \times (\mathbf{E} \exp(in\phi))] + \mathbf{F}^*_{j,k} \cdot \boldsymbol{\varepsilon} \cdot \mathbf{E} + i\frac{\omega}{c^2} \mathbf{F}^*_{j,k} \cdot \mathbf{j}_{e,n}\} = 0 \,. \tag{5}$$

Substitution of Eq. (4) into Eq. (5) yields a sparse matrix system that is amenable to solution by standard algorithms. Wave amplitude, Poynting flux, and wave polarization are all

obtained from the resulting solutions. From these wave solutions, it is possible to estimate the amount of mode conversion between propagating modes and absorption near resonances.

One advantage of using the finite element method is that the local basis functions that are employed can be readily adapted to boundary shapes and can be packed in such a way as to provide higher resolution in regions where solutions may exhibit singular behavior. We have adapted the DISTMESH algorithm developed by *Persoon and Strang* [2004] to a magnetospheric geometry. The algorithm constructs a 2D triangular or 3D tetrahedral mesh given a specified boundary and a target density function. Where the geometry is more complex (near the boundary and near singularities) the wave solution needs to be resolved by small elements to give good global accuracy. Moreover, the density of the mesh can be specified based on the expected wavelength obtained from solution of the local dispersion (except close to resonances) so that the most efficient resolution is used. This mesh algorithm is particularly useful because it allows us to pack extra resolution near singular regions where mode conversion occurs. As examples, the cyclotron resonances and Buchsbaum [*Buchsbaum*, 1960] resonances depend on magnetic field strength while the Alfvén and ion-ion hybrid resonances [*Lee et al.*, 2008] are field-aligned resonances. They can both be relevant for magnetosonic wave propagation, but are not well suited to any particular coordinate system. However, with the finite element approach, high grid resolution can be placed along a particular field line region for the Alfvén resonance or along surfaces of magnetic field strength for the Buchsbaum resonance or optimized to resolve both resonances. These properties of the finite element mesh provide significant advantages over wave codes based on the finite difference technique or methods tied to any particular coordinate system. In the cold plasma model, resonances are resolved by a small collisional term introduced near the resonance location, and the total energy absorption should be independent of the collision frequency in that limit. This approach gives reasonable estimates of wave power losses near the Alfvén and cyclotron resonances when particle Doppler shifts are not large, although the physical dissipation process is not known.

3. RESULTS FROM THE FINITE ELEMENT CODE

3.1. Magnetosonic Wave Propagations

As an example of the utility of our code, we have examined two-dimensional propagation of magnetosonic waves in a realistic magnetospheric geometry considering the effects of a plasmaspheric plume on wave propagation. For the field, we have taken a dipole (but an arbitrary field can be specified as we are not tied to any coordinate system). The inner magnetospheric density model used in this calculation is based on the observational study of *Denton et al.* [2004, 2006], while a background density of $1cm^{-3}$ is imposed in the outer magnetosphere. Reflecting boundary conditions are prescribed at the earth's surface, while absorbing boundary conditions are prescribed at all other boundaries. A large-scale compressional wave is launched at 8 RE in the model and propagates away from the source both earthward and tailward (the tailward traveling wave propagates to the boundary where it is absorbed so it does not affect the solution in the inner magnetosphere). We consider cases with and without a density plume localized near L = 5.5. The Alfvén velocity profile with the plume is shown in the left panel of Figure 1 along with the finite element mesh. The plume provides a local reduction in the Alfvén speed. The mesh density is selected to optimize the resolution of the wave structure using the local phase velocity as a guide for the element size. Because compressional waves refract away from the gradient of the Alfvén velocity, the wave will be refracted into the plume. The right panel of Figure 1 shows the wave solution along with several ray paths obtained with a ray tracer. The ray paths provide a nice confirmation of the general behavior of the solutions and how the wave fronts refract. As waves propagate into the inner magnetosphere they are refracted away from the earthward Alfvén velocity gradient leading to enhanced wave power at the equatorial plasmaspheric boundary. It is apparent from the Finite Element Model solution, that wave energy is trapped in the Alfvén velocity well and forms a leaky eigenmode-like structure. Therefore, the finite element approach provides a more complete description of wave amplitude and structure than can be obtained from the ray-tracing approach alone.

Trapping of wave energy in the plasmaspheric plume also affects how much magnetosonic wave power can reach the plasmaspheric boundary (where wave energy accumulates as the wave reflects). Figure 3 illustrates significant differences in the wave

power with (right panel) and without (left panel) the plasmaspheric plume. It is evident that the plasma plume sucks in the wave energy shadowing the plasmaspheric boundary from the pile-up of wave energy seen in the case without the plasma plume (left panel). The reduction in wave power reaching the plasmaspheric boundary when a plasmaspheric plume is present could be an important effect because magnetosonic waves are relevant for energization of radiation belt electrons.

3.2. Alfven Resonance

We also perform the Alfven resonance which is one of the interesting wave coupling problems in the Earth magnetosphere. In this case, we adopt the cylindrical coordinate system. The magnetic field lies in z-direction and changed in radial direction $\boldsymbol{B}_0 = B_{0z}$ (r). For simplicity, we adopt a uniform density in the code and the Alfven velocity and resonant frequency decrease in radial direction as shown in Figure 3(a). Figure 3(b) shows the full wave solutions for a $\omega = 0.11\omega_{ci}$ launched at 5.5 RE. Here E_{radial} and $E_{azimuthal}$, are transverse and compressional wave components, respectively. E_{radial} shows enhanced wave power near the 3.1 RE which is resonant location shown in (a). We also examine the wave Poynting flux (not shown) and field-aligned Poynting flux is dominant. These are the evidence of Alfven resonance.

The computational results shown require about 10 seconds for compressional wave calculations and several minutes for Alfven resonance calculation on a single processor. To take advantage of the sparseness of the matrix system, we have employed a Gibbs algorithm to reorder the mesh to minimize the bandwidth of the matrix. Because of the size of the matrix required to adequately resolve the modes discussed in this proposal, we have already parallelized the code using the ScaLAPACK algorithm. The parallelized code has been tested with the propagation of magnetosonic waves in a dipole field and with the Alfvén resonance and are found to be consistent with the single processor solutions.

4. FUTURE WORK

In the near future, in order for our code to be even more useful to inner magnetospheric transport models, we would extend our model to also describe three-dimensional background plasma and magnetic field configurations and include kinetic damping and Larmor radius physics.

4.1. Extension to a three-dimensional quasi-equilibrium configuration

Although, our code does account for three-dimensional structure in the perturbed wave fields, it currently assumes axisymmetric background plasma and magnetic field profiles. To be even more practicable for addressing transport, it would be useful to extend our approach to describe wave propagation in three-dimensional background configurations, which leads to coupling in the azimuthal modes described in Eq (3). For large-scale asymmetries in the inner magnetosphere (such as compression of dipole field, dawn-dusk asymmetries, day-night asymmetries or plasmaspheric asymmetry) it is efficient to retain the global Fourier basis functions in which case Eq (5) is generalized to include coupling between azimuthal numbers, but the number of modes that are coupled is relatively small for large-scale inhomogeneity in the azimuthal direction. This extension is straightforward to implement without much additional computational cost.

For smaller-scale azimuthal gradients that might arise when there are plasma plumes or when there is azimuthal dependence in resonant surfaces, we can use three-dimensional tetrahedral finite elements. Extension from triangular mesh to tetrahedral mesh is straightforward to implement (DISTMESH also creates a three-dimensional mesh), and we would use the cubic element basis functions discussed in section 2. The overlap integrals are obtained analytically and the matrix can be loaded by evaluating the cold dielectric tensor and its derivatives at the center of each tetrahedron. Once the matrix is loaded, sorting and inversion of sparse matrix would be accomplished as in the two-dimensional case. The primary task that needs to be accomplished is to compute and load the overlap integrals from the weak variational form.

The extension to three dimension will allow us to further address asymmetries in the distribution of externally driven ULF waves, EMIC waves, and magnetosonic waves that result from azimuthal asymmetries in the background plasma model. We would plan to use plasma and magnetic field profiles obtained from the MAG3D equilibrium code [*Cheng*, 1995].

4.2. Including parallel kinetic effects

Whereas adapting a finite difference multi-fluid wave code to include kinetic effects would require a major overhaul in the numerical scheme, including kinetic effects in the full-wave model is relatively straightforward because finite-element methods are well suited

to solve integral equations such as Eq (5). When kinetic effects are included, the Maxwell system of equations are modified because the plasma response includes contributions from the past history of the particle orbits, such that

$$\mathbf{J}(x) = \int \sigma(x, x') \cdot \mathbf{E}(x') dx' \tag{6}$$

The form of the kernel $\sigma(x, x')$, has been described in detail by *Brambilla* [1999]. This plasma response contributes to the local dielectric tensor **ε** used in Eq (1). With the finite element approach, it is necessary to compute the kernel in real space, and we have substantial experience doing this in fusion plasmas where it is necessary to model Landau and cyclotron resonance as well as Larmor radius effects. The form of the conductivity kernel to describe Landau damping has been computed by *Lysak and Song* [2003] in the context of a nonlocal kinetic theory of Alfvén waves. The kernel is evaluated assuming a bi-Maxwellian distribution and integrating over velocity space. Similarly, the nonlocal response at the cyclotron resonance can also be described with a nonlocal modification to the conductivity involving the coordinate parallel to the magnetic field [*Johnson and Cheng*, 2010]. As an example, the equivalent local ion cyclotron resonance operator assuming a bi-Maxwellian distribution takes the form

$$\frac{\delta(z-z')}{\omega-\Omega} \rightarrow \int_0^\infty \frac{dv_z}{v_z} f_0(v_z) \exp\left(i(\omega - \overline{\Omega}) \frac{|z-z'|}{v_z} \right) = \frac{1}{\sqrt{2}v_t} f_\alpha(\Delta) \; ; \; \Delta = \frac{\omega - \overline{\Omega}}{\sqrt{2}v_t} |z-z'| \tag{7}$$

where the equivalent resonance function is

$$f(\Delta) = \frac{-i}{\sqrt{\pi}} \int_0^\infty \frac{dp}{p} \exp(ip\Delta - p^{-2}) \tag{8}$$

The function, *f*, approaches a delta function in the low temperature limit, and can be evaluated numerically by the method of steepest descents and tabulated for use from a lookup table when performing the integration over the field-aligned coordinate. When the overlap integrals are constructed, this resonance operator couples elements that are within roughly a distance $v_{t\|} = \Omega$ of the region of resonant interaction, so the matrix is not quite as sparse, but is manageably inverted within the two-dimensional implementation of the code.

With these improvements, we can address EMIC and magnetosonic wave growth based on anisotropic or ring (subtracting Maxwellians) distributions. We can also address electron Landau damping of chorus waves, so we can examine the radial and latitudinal extent of the waves and the development of plasmaspheric hiss near the magnetospheric boundary.

4.3. Including Larmor radius physics

Finite Larmor Radius (FLR) corrections may also be included through the expansion of the nonlocal plasma response (Eq (6) to second order in ion gyroradius so that the wave equation becomes fourth order). Such expansions are regularly used in fusion plasma codes and have been solved in the ion cyclotron range of frequencies using massively parallel processing computers to study mode conversion of long wavelength fast magnetosonic waves into short wavelength ion Bernstein waves [*Brambilla*, 1999; *Wright et al.*, 2004]. These have also been used to model mode conversion processes in the magnetosphere [*Johnson and Cheng*, 1997; *Johnson et al.*, 2001]. Essentially, the higher order derivative terms that are introduced through the FLR expansion represent the short wavelength mode converted waves. By replacing these higher order derivatives with appropriate powers of an effective $k_\perp$, derived for the longer wavelength mode from the full local FLR dispersion relation, the order of the system of equations to be solved remains the same as in the cold plasma case, but the net amount of plasma absorption and mode conversion is now included through the anti-Hermitian part of the truncated warm plasma dielectric operator. One does lose all information on the spatial structure of the mode converted waves with this reduced order approach, but the effects of the mode conversion on the total absorption can be included with reasonable accuracy and with less computational requirements. The accuracy of the 2D FLR code can be validated against 1D kinetic models for the mode conversion interactions, as done for fusion plasmas [*Snipes et al.*, 2000].

The primary motivation for us to include Larmor radius effects in our model is to be able to describe damping of EMIC waves at the cyclotron harmonics. Harmonic damping has been found to be important in hybrid simulations [*Hu et al.*, 2010] and ray tracing calculations [*Horne and Thorne*, 2000; *Horne et al.*, 2007]. We would be able to compare with these previous model results and understand better how harmonic damping could heat ions and dissipate wave energy.

5. SUMMARY

Many plasma waves play an important role in energization and loss of radiation belt electrons and ring current particles that are injected from the plasma sheet [*Thorne*, 2010]. We develop a finite element code to understand the distribution of wave power and

characteristics of the waves that are relevant for transport calculations. In its current, two-dimensional form, it can describe propagation and mode conversion of ULF, EMIC, magnetosonic, and whistler waves. In the future, we will adapt the code to solve the wave equations for a given three-dimensional quasi-equilibrium configuration to examine asymmetries in ULF, EMIC, magnetosonic, and whistler wave power distribution. By including a kinetic plasma response, we can also address the wave generation mechanisms and kinetic damping that limit their spatial extent, which are outstanding issues that are critical for accurate modeling of the radiation belts and ring current.

Acknowledgements

The work was supported by NASA grants (NNH09AM53I, NNH09AK63I, and NNH11AQ46I), NSF grant ATM0902730, and DOE contract DE-AC02-09CH11466.

References

Bonoli, P. T., et al., Physics Research in the SciDAC Center for Wave-Plasma Interactions, in Radio Frequency Power in Plasmas, American Institute of Physics Conference Series, vol. 933, edited by P. Ryan & D. Rasmussen, pp. 435-442, doi:10.1063/1.2800525, 2007.

Brambilla, M., Numerical simulation of ion cyclotron waves in tokamak plasmas, Plasma Physics and Controlled Fusion, 41, 1-34, doi:10.1088/0741-3335/41/1/002, 1999.

Buchsbaum, S. J., Resonance in a Plasma with Two Ion Species, *Phys. Fluids*, 3, 418-420, 1960.

Chen, Y., R. H. W. Friedel, G. D. Reeves, T. E. Cayton, and R. Christensen, Multisatellite determination of the relativistic electron phase space density at geosynchronous orbit: An integrated investigation during geomagnetic storm times, *J. Geophy. Res.*, 112, 11,214, doi:10.1029/2007JA012314, 2007.

Denton, R. E., J. D. Menietti, J. Goldstein, S. L. Young, and R. R. Anderson, Electron density in the magnetosphere, *J. Geophys. Res.*109 (A18), 09,215, doi:10.1029/2003JA010245, 2004.

Denton, R. E., K. Takahashi, I. A. Galkin, P. A. Nsumei, X. Huang, B. W. Reinisch, R. R. Anderson, M. K. Sleeper, and W. J. Hughes, Distribution of density along magnetospheric field lines, *J. Geophys. Res.*, 111 (A10), 04,213, doi:10.1029/2005JA011414, 2006.

Horne, R. B., and R. M. Thorne, Electron pitch angle diffusion by electrostatic electron cyclotron harmonic waves: The origin of pancake distributions, *J. Geophys. Res.*, 105, 5391-5402, doi:10.1029/1999JA900447, 2000.

Horne, R., R. Thorne, S. Glauert, N. Meredith, D. Pokhotelov, and O. Santolík, Electron acceleration in the Van Allen radiation belts by fast magnetosonic waves, *Geophys. Res. Lett.*, 34, L17,107, doi:10.1029/2007GL030267, 2007.

Hu, Y., R. E. Denton, and J. R. Johnson, Two-dimensional hybrid code simulation of electromagnetic ion cyclotron waves of multi-ion plasmas in a dipole magnetic field, *J. Geophys. Res.*, 115, 9218, doi:10.1029/2009JA015158, 2010.

Johnson, J. R., and C. Z. Cheng, Kinetic Alfvén waves and plasma transport at the magnetopause, *Geophys. Res. Lett.*, 24 (11), 1423-1426, doi:10.1029/97GL01333, 1997.

Johnson, J. R., and C. Z. Cheng, Kinetic effects in ion cyclotron wave mode conversion in a multi-ion plasma, to be submitted to J. Geophys. Res., Preprint at w3.pppl.gov/ jrj/icw.html, 2010

Johnson, J. R., C. Z. Cheng, and P. Song, Signatures of Mode Conversion and Kinetic Alfvén Waves at the Magnetopause, *Geophys. Res. Lett.*, 28 (2), 227-230, doi:10.1029/2000GL012048, 2001.

Kim, E.-H., J. R. Johnson, and D. Lee, Resonant absorption of ULF waves at Mercury's magnetosphere, *J. Geophys. Res.*, 113, 11,207, doi: 10.1029/2008JA013310, 2008a.

Lee, D., J. R. Johnson, K. Kim, and K. Kim, Effects of heavy ions on ULF wave resonances near the equatorial region, *J. Geophy. Res.*, 113, 11,212,doi:10.1029/2008JA013088, 2008.

Persson, P.-O., and G. Strang (2004), A Simple Mesh Generator in MATLAB. SIAM Review, Volume 46 (2), pp. 329-345.

Reeves, G. D., A. Chan, and C. Rodger, New Directions for Radiation Belt Research, *Space Weather*, 7, 7004, doi:10.1029/2008SW000436, 2009.

Snipes, J. A., A. Fasoli, P. Bonoli, S. Migliuolo, M. Porkolab, J. E. Rice, Y. Takase, and S. M.Wolfe, Investigation of fast particle driven modes on Alcator C-Mod, Plasma Physics and Controlled Fusion, 42, 381-388, doi:10.1088/0741-3335/42/4/301, 2000.

Stix, N., Waves in plasmas, American Institute of Physics, New York, 1992.

Thorne, R. M., Radiation belt dynamics: The importance of wave-particle interactions, *Geophys. Res. Lett.*, 37, L22,107, doi:10.1029/2010GL044990, 2010.

Wright, J. C., et al., Full wave simulations of fast wave mode conversion and lower hybrid wave propagation in tokamaks, *Phys. Plasmas*, 11, 2473-2479, doi:10.1063/1.1652731, 2004.

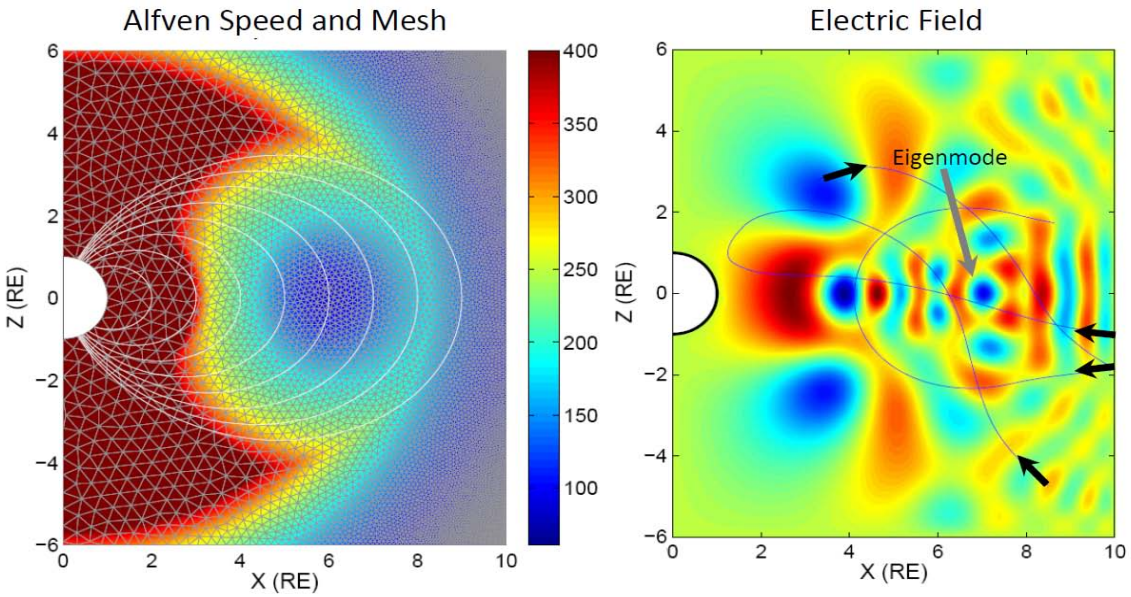

Figure 1. *Left*: Alfvén speed profile and finite element mesh using a plasma density model prescribed by *Denton et al.* [2004] with the addition of a plasmaspheric plume added at 5.5 RE. *Right*: full wave solutions for a 0.1 Hz magnetosonic wave launched at 8 RE showing wave trapping in the plume and associated ray paths

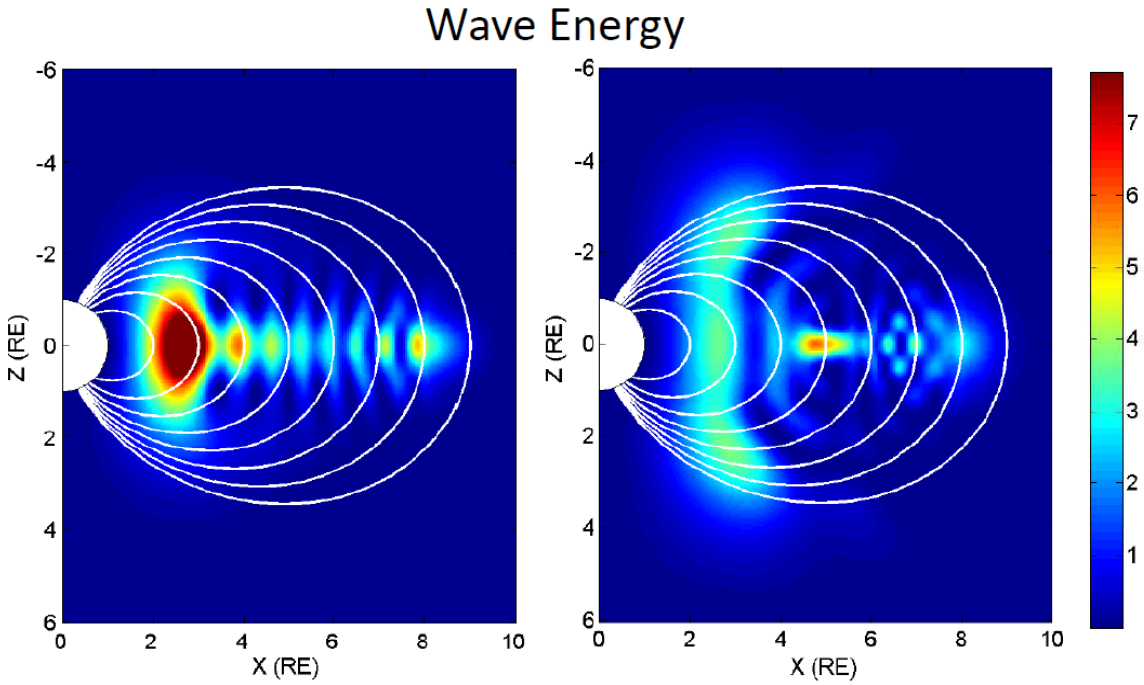

Figure 2. Wave power of wave solutions for a 0.1 Hz magnetosonic wave launched at 8 RE. Without a plasmaspheric plume (left) wave power maximizes near the plasmaspheric boundary where the wave reflects. A plasmaspheric plume traps wave power so that wave energy is trapped in the plume (right) rather than maximizing at the plasmaspheric boundary.

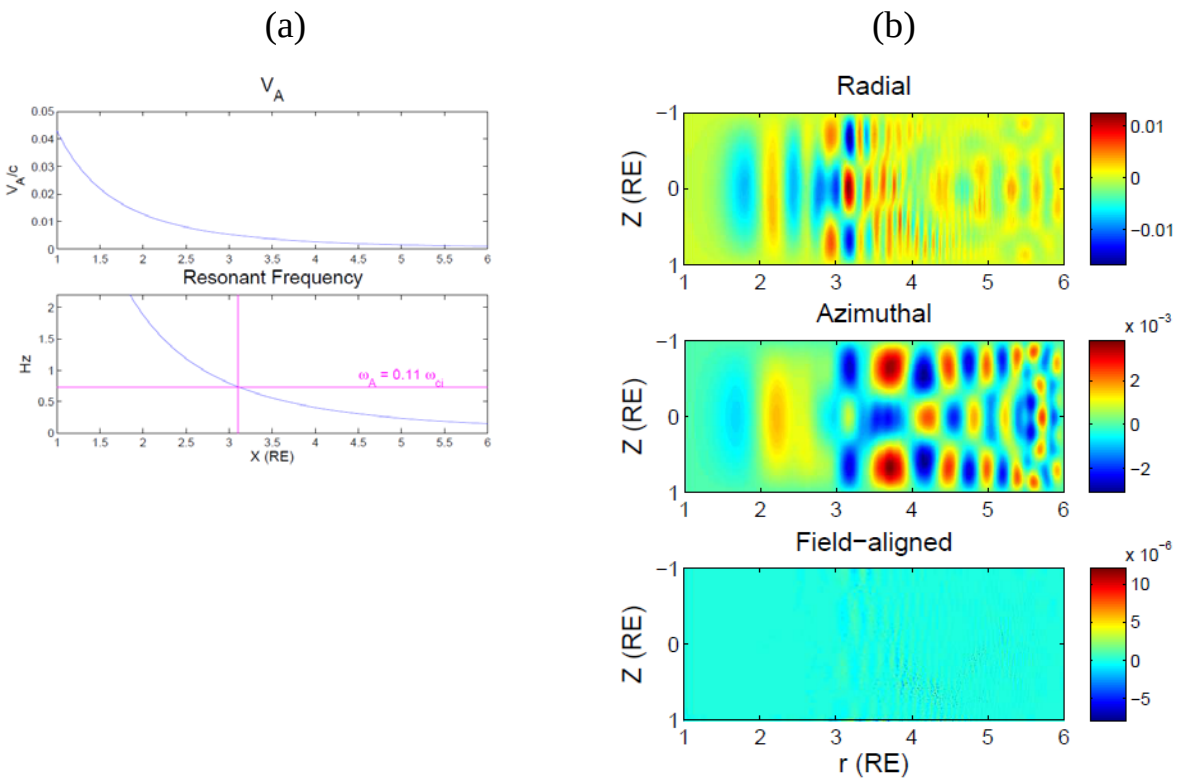

Figure 3. (a) *Left*: Alfvén speed profile and Alfvén resonant frequencies in the radial direction. *Right*: (b) Full wave solutions for a $\omega = 0.11\omega_{ci}$ launched at 5.5 RE. Here E_{radial} and $E_{azimuthal}$, are transverse and compressional wave components, respectively. E_{radial} shows enhanced wave power near the 3.1 RE which is resonant location shown in (a). We use cylindrical coordinate in this calculation.

The Princeton Plasma Physics Laboratory is operated
by Princeton University under contract
with the U.S. Department of Energy.

Information Services
Princeton Plasma Physics Laboratory
P.O. Box 451
Princeton, NJ 08543

Phone: 609-243-2245
Fax: 609-243-2751
e-mail: pppl_info@pppl.gov
Internet Address: http://www.pppl.gov